

The Effect of Different Precursor Solutions on the Structural, Morphological, and Optical Properties of Nickel Oxide as an Efficient Hole Transport Layer for Perovskite Solar Cells

Subathra Muniandy^{1*}, Muhammad Idzdihar Idris¹, Zul Atfyi Fauzan Mohammed Napiah¹, Nurbahirah Norddin¹, Marzaini Rashid², Ahmad Wafi Mahmood Zuhdi³ and Luke Bradley⁴

¹Faculty of Electronics and Computer Engineering, University Technical Malaysia Melaka, 75450 UTeM, Melaka, Malaysia

²School of Physics, University Science Malaysia, 11800 USM, Penang, Malaysia

³Department of Electrical & Electronic Engineering, Universiti Tenaga Nasional, 43000 UNITEN, Selangor, Malaysia

⁴School of Engineering, Newcastle University, England

ABSTRACT

Perovskite solar cell (PSC) technologies have recently become a popular research topic. The hole transport layers (HTL) are important in establishing stable and efficient PSC by regulating charge absorption, interlayer recombination losses, and band alignment. Spiro-OMeTAD was extensively used as the HTL to fabricate highly efficient PSCs. Despite Spiro-OMeTAD having the benefit of providing high PCEs, it is costly, hazardous to the ecology, and cannot provide high efficiencies in the lack of additional additives that can reduce their stabilities. Inorganic HTL, specifically nickel oxide (NiO), has garnered much interest due to its low-cost, enhanced mobility, and strong stability to attain high efficiency.

This study investigated different precursor solutions of NiO synthesis (Method I, II, and III) and deposited using the spin coating approach. The films were annealed at different annealing temperatures (400°C, 550°C, and 700°C) and evaluated by X-ray powder diffraction (XRD), UV-Vis spectroscopy, and Scanning electron microscopy (SEM) to test their structural, morphological, and optical characteristics, respectively. The findings of XRD revealed that a higher annealing temperature increases

ARTICLE INFO

Article history:

Received: 22 July 2022

Accepted: 02 November 2022

Published: 13 June 2023

DOI: <https://doi.org/10.47836/pjst.31.4.26>

E-mail addresses:

m022020016@student.utem.edu.my (Subathra Muniandy)

idzdihar@utem.edu.my (Muhammad Idzdihar Bin Idris)

zulatfyi@utem.edu.my (Zul Atfyi Fauzan Bin Mohammed Napiah)

nurbahirah@utem.edu.my (Nurbahirah Binti Norddin)

marzaini@usm.my (Marzaini Rashid)

wafi@uniten.edu.my (Ahmad Wafi Bin Mahmood Zuhdi)

luke.bradley@newcastle.ac.uk (Luke Bradley)

* Corresponding author

the crystallite size and decreases the microstrain through the study from Scherrer's and Williamson-Hall's (WH) equations. From the SEM analysis, the films show uniformity, large crystals, and agglomeration of particles. The annealing temperature from 400°C to 700°C reduced bandgap energy from 3.6 eV to 2.1 eV. According to the result, NiO produced at an annealing temperature of 700°C (Method I) exhibited the best characteristics and might be a viable option for HTL in PSCs.

Keywords: Hole transport material, nickel oxide, perovskite solar cells, spin coating

INTRODUCTION

Solar energy is one of the renewable sources that can support the world's increasing energy demand and address the emerging energy crisis caused by the depletion of fossil fuels. In comparison with nuclear technology, the worldwide spreading of sunshine (unlike the wind, geothermal, or hydropower sources in particular regions) and the lack of dangerous waste creation, and the decentralization of energy generation are the major advantages over many other renewable energy sources (Mohammadian-Sarcheshmeh et al., 2020), (Du John H et al., 2020). Photovoltaic solar cells function by transforming energy into electrical energy from incoming photons. Numerous photovoltaic approaches have been developed in three generations (Younas et al., 2019). Regarding the various 3G solar cell technologies research, perovskite solar cells (PSCs) are now the technology that develops most fast (Abbas et al., 2020; Gil et al., 2019; Ibn-Mohammed et al., 2017; Nkele et al., 2020). Recently, PSCs have globally pushed conventional solar cell methods for resolving global energy production, safety, and environmental issues as a cost-effective (Haider et al., 2019) and environmentally feasible renewable technology choice (Ebhotu & Jen, 2020; Mariotti et al., 2020; Roy et al., 2020; Wilson et al., 2020). Ever since this finding, PSCs have been researched intensively for the last five years with their distinctive features like large absorption coefficients, open-circuit voltage (V_{oc}) (Wang et al., 2017), and long load carrier (electron-hole) diffusion length (Wang et al., 2019). Perovskite absorbers are also desirable because they are simple to solution-process at low temperatures with low-cost chemicals and do not rely on components in limited supplies, unbalanced solvents like hydrazine, or high-temperature processing (Pitaro et al., 2022; Yang et al., 2020)

PSCs are typically made up of charge transport layers called electron transport layers (ETL) and hole transporting layers (HTL) that interface with the perovskite material for efficient and selective charge absorption (Łuszczek et al., 2021) (Yin et al., 2019). Detailed attention was paid to the HTL layer concerning the PSC design. The materials used for HTL have a major influence on the performance of PSCs. One of the most popular HTLs in PSCs was Spiro-OMeTAD. As a result, the impedance and the interfacial recombine loss in PSCs are minimized, enabling to improve of PSCs' fill factor (FF) and open-circuit

voltage (V_{oc}), apart from efficiency in the transmission of holes to the counter electrode (Gil et al., 2019). Even though PSCs based on Spiro-OMeTAD have better power conversion efficiencies (PCEs), high costs for Spiro-OMeTAD remain important barriers in marketing PSCs owing to the extensive and poor productivity synthetic methodology (Shariatnia, 2020). To enhance the innate conductivity and hole mobility of Spiro-OMeTAD (Wang et al., 2017), which also raises the manufacturing cost of PSCs containing Spiro-OMeTAD, ionic addition products like bis(trifluoromethane) sulfonamide lithium salt (Li-TFSI) and 4-tert-butyl pyridine (TBP) and co-doping are also to be added. Due to their inherently high selectivity, high ion charge mobility, and cheap overall cost, some inorganic substances are investigated as HTLs (Hajakbari et al., 2017). In addition, several inorganic hole transport materials (HTM) such as copper thiocyanate (CuSCN), copper iodide (CuI), copper oxide (CuO), cuprous oxide (Cu₂O), and nickel oxide (NiO) are studied for PSCs. Inorganic materials, which can be acquired at a considerably lower cost than organic materials, are considered to have a better possibility of becoming a major role in solar cell technology due to the stability of their structures in the face of environmental factors, including humidity, light, and temperature stress.

Although organic HTL materials provide great potential, it can be argued that inorganic materials, with the refinement of their manufacturing methods, have more potential to overcome present impediments in commercialization. Copper-based inorganic semiconducting HTM has demonstrated potential for use in dye- and quantum dot-sensitized solar cells. The solution technique to deposit these materials ensures that the pores are filled, and the resulting broadband gap semiconductors exhibit excellent conductivity, an appropriate energy level, and great transparency (Li et al., 2016). However, structures containing copper-based inorganic materials have demonstrated poor efficiency and stability problems (Nkele et al., 2020). Experts explored how inorganic materials, especially NiO, a p-type HTL, are used in organic solar and dye-sensitized solar cells (DSSC) to overcome this problem. Numerous research institutions have actively studied DSSCs due to their cheap manufacturing cost, non-toxicity, and potential for strong energy conversion efficiencies (Atli et al., 2019; Atli et al., 2018).

For the development of DSSCs, it is important to develop a counter electrode (CE) material with outstanding catalytic activity, inherent stability, and cheap cost (Yildiz et al., 2021). It is because sensitizing a p-type material with broadband content, such as NiO, could help the interfacial charge-carrying behavior of perovskites and is thus vital to forming wide-range device topologies that were noticed since closer exploring into NiO HTL. NiO is recognized as a p-type semiconductor with a broad energy bandgap (3.2 to 4.0 eV) and has considerable promise as a catalyst for replacing Spiro-OMeTAD owing to its outstanding features including cheap cost materials, nontoxicity, physical-chemical stability, and strong iodine-based catalyst function (Gil et al., 2019), [17]. NiO is a substance

that is extremely resistant to thermal and chemical processing and improves the strength of PSCs, among several other inorganic hole transporters. In this study, the influence of NiO was explored in three different methods by synthesizing with varying precursor solutions. The NiO was deposited using a spin-coating procedure and annealed at different annealing temperatures (400°C, 550°C, and 700°C). The resultant films were then examined to study the morphological, structural, and optical characteristics of NiO using Scanning Electron Microscopy (SEM), X-ray diffraction (XRD), and UV–vis spectroscopy, respectively.

HTM is important in collecting holes (positive charges) from the absorber material following excitation and directing such charges toward the active electrode. Since HTMs are anticipated to enhance the functionality of devices, they were developed to substitute the dye in a DSSC and create a solid solar cell (Nkele et al., 2020). In conjunction with better performance and durability, a low-cost manufacturing method with strong heat and humidity resistance is crucial for achieving a marketable dimension. An ideal HTM candidate features inherently high hole mobility, an appropriate energy level, long-term stability in the air, and excellent photochemical and thermal durability. Additionally, it must be solution-processed to create HTL, particularly when used in typical (n-i-p) PSCs. Consideration must also be given to the low cost and simplicity of HTM preparation for manufacture on a large scale and additional commercial applications (Li et al., 2021; Park, 2021).

METHODOLOGY

Material and Preparation

Nickel acetate tetrahydrate (purity, 98%) and diethanolamine (DEA) were bought from the Sigma Aldrich website. Besides that, nickel oxide powder, ethanol (purity, 95%), potassium hydroxide, and isopropyl alcohol (IPA) were purchased from Chemiz (M) Sdn Bhd. Deionized water was used to prepare all aqueous solutions. The substrates of ITO glass and beakers were washed with a detergent one by one and dried in the ultrasound bath with IPA, ethanol, and deionized water to eliminate pollution and strain on the surface. This study synthesized and coated three different precursor solutions (Methods I, II, and III) by spin coating techniques on the ITO glass substrate. The sample of NiO films was then annealed at various temperatures (400°C, 550°C, and 700°C).

Syntheses of NiO (Method I)

0.622 g nickel acetate tetrahydrate was dissolved in ethanol (15 ml) and IPA (10 ml). Afterward, potassium hydroxide (0.56 g), mixed with distilled water (100 mL), was dropped into the solution till the pH of the mixture was attained at level 10, as seen in Figure 1. The solution was then mixed on the hot plate. The resulting solution in greenish color is

refined by rinsing the unreacted chemicals over five times using ethanol. The concentrated solution was then dried and placed in the oven for 1 hr. The resulting powder of NiO was then acquired to continue the coating procedure and characterization.

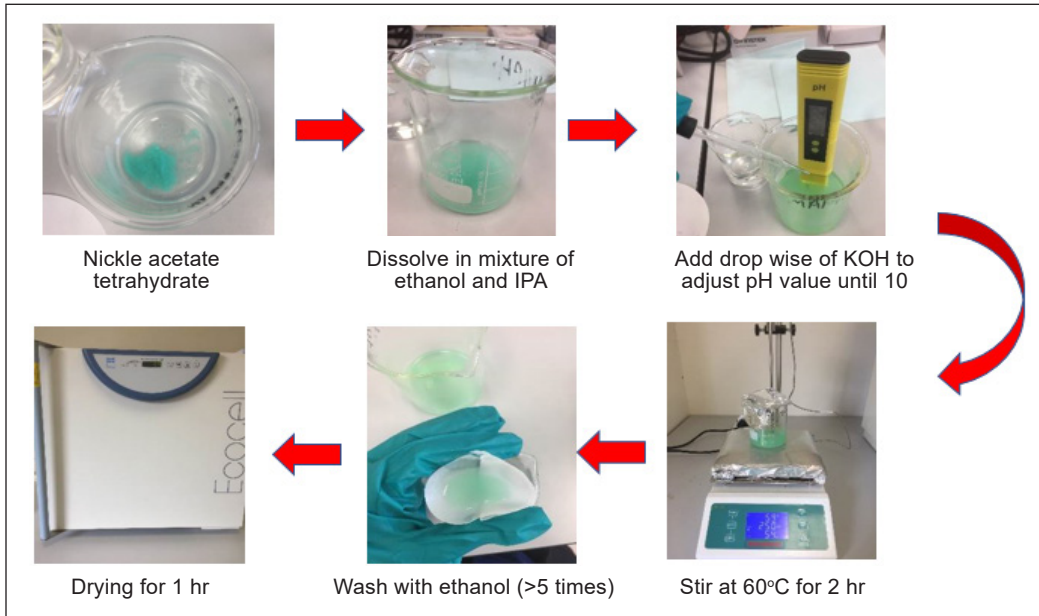


Figure 1. Schematic representation of Method I for synthesizing NiO using nickel acetate tetrahydrate, ethanol, and potassium hydroxide

Synthesis of NiO (Method II)

Nickel acetate tetrahydrate, ethanol, and DEA were employed as solutes, solvents, and stabilizers. First, 0.1 M nickel acetate was mixed in ethanol and agitated for 2 hr to a pure and uniform mixture at 60°C on a hot plate (Figure 2). In the agitation, DEA dropwise was added to the mixture. To avoid aggregation or agglomerations, the function of DEA

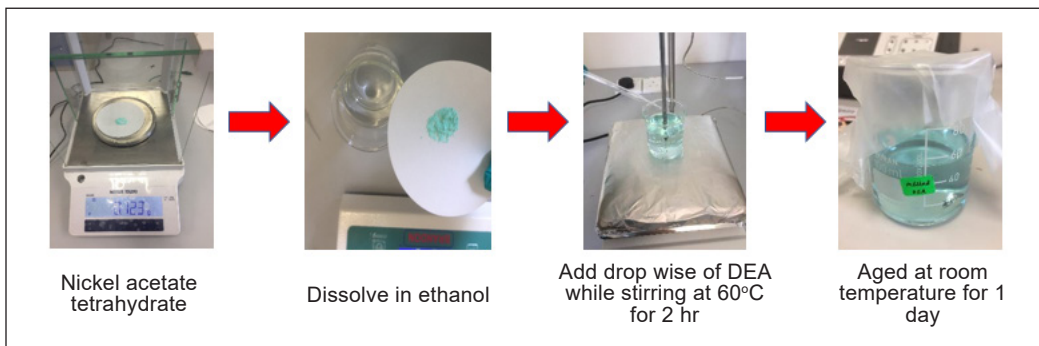


Figure 2. Schematic representation of Method II for the synthesizing NiO nickel acetate tetrahydrate, ethanol, and DEA

works as a stabilizing agent and increases hydrolysis stability. The nickel acetate molar ratio to DEA was maintained at 1:1. The mixture was then stored for a whole day at room temperature to enhance its consistency and transform it into a concentrated solution.

Synthesis of NiO (Method III)

NiO powder purchased from Chemiz was just 40 ml ethanol diluted and sonicated for 15 minutes (min) to maintain that the NiO powder in ethanol was dissolved thoroughly. The NiO was then utilized with the spin coater for the additional coating procedure. The three different synthesis methods of NiO are summarized in Table 1.

Table 1
A comparison between three different methods (I, II, and III)

Method	Precursor
I	Nickel acetate tetrahydrate, ethanol, isopropyl alcohol, potassium hydroxide, and distilled water
II	Nickel acetate tetrahydrate, ethanol, and DEA
III	NiO powder, ethanol

Deposition of NiO Thin Film

Disposing of NiO covered by spin-coating techniques on ITO glass substrates. At 3000 rpm/s acceleration, the NiO produced was treated by a spin-coater for 30 sec. After spins,

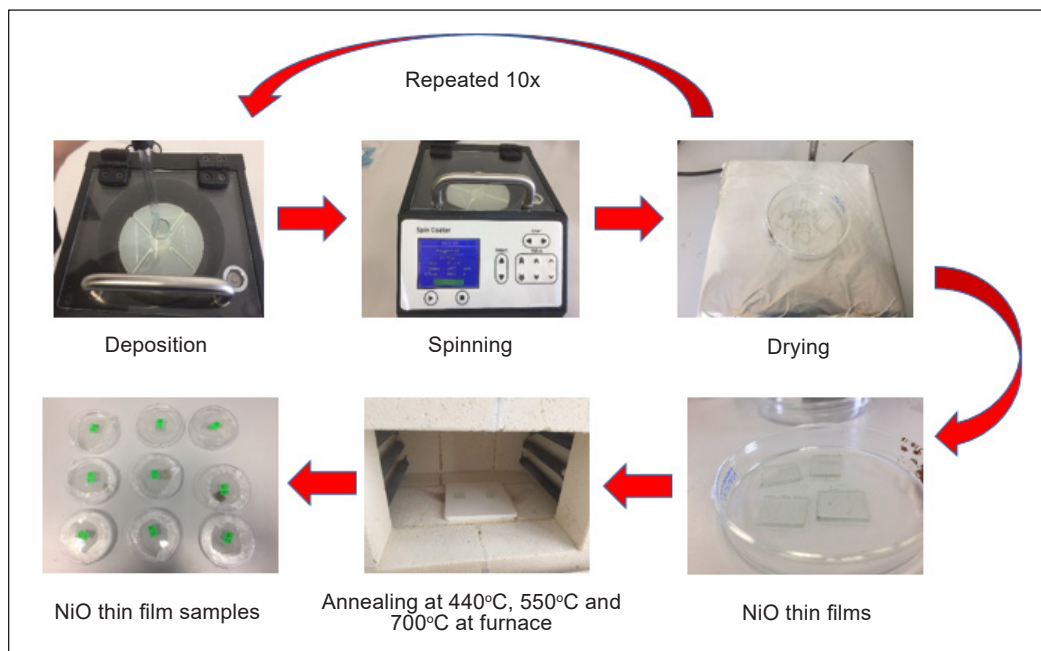


Figure 3. Illustration for deposition of NiO using spin coating technique for every specimen in all the methods (Methods I, II, and III)

organic residues were evaporated on a thermal plate for 15 minutes (min). The coating and drying processes were performed for 10 cycles for every specimen to boost the thickness of the NiO layer. The samples were progressively rinsed in ambient conditions for 400°C, 550°C, and 700°C for 1 h. The thin NiO films were finally obtained, as illustrated in Figure 3. The structural characteristics were defined by X-rays Powder Diffraction (PANalytical system) fitted with Cu K α (0.154056 nm) scanning, which was supplied by a (θ -2 θ) scan of each NiO thin film. A scanning electron microscope (SEM) performed surface morphology. To analyze the morphology of the film, a gold coating was applied to produce a uniform surface for SEM investigation analysis and imaging. The absorbance of the films was measured using a Shimadzu UV-1800 spectrophotometer within the wavelength range of 200 to 900 nm.

RESULT AND DISCUSSION

Structural Analysis

Figure 4(a) shows the XRD pattern of NiO thin films from Method I at three different temperatures. The XRD pattern of the NiO film at 400°C and 550°C only showed two prominent peaks at 37.2° and 79.3°, that is, (1 1 1) and (2 2 2) diffraction of the cubic NiO diffraction planes (ICDD 00-044-1159). The NiO film at 700°C shows well-defined spread peaks at 37.2°, 43.3°, 68.2°, 75.2° and 79.4° which correspond to (1 1 1), (2 0 0), (2 2 0), (3 1 1), and (2 2 2). No secondary peaks indicated that the Ni was fully oxidized, and no NiO formation by-products were detected (Desissa, 2021; Muniandy et al., 2021). Based on the XRD, the intensity of every diffraction peak increased as the temperature increased, and therefore the peak went sharper from 400°C to 700°C, which is also an equivalent statement made (Guo et al., 2017). It was also in conjunction with the studies of Temesgen D. Desissa (Desissa, 2021), who discovered that temperatures exceeding 700°C (about 900°C) lead to an XRD pattern, which suggested that the interface remains stable with no more phases. Evidently, with the increase in temperature, the strength of all spikes was enhanced. It indicates that NiO films can enhance their crystalline quality by increasing temperature. All NiO films showed the highest intensive diffraction peak and were orientated at (111). Scherrer's equation (Equation 1) was applied to measure the average crystallite size:

$$D = 0.9\lambda / \beta \cos \theta \quad [1]$$

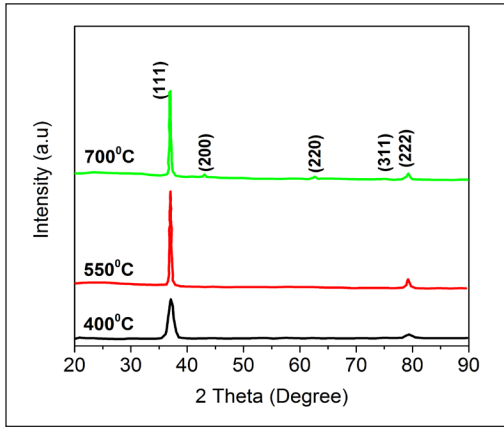
where D is the crystallite size (nm), λ is the incident wavelength, β is the half-width of the diffraction peak quantified in radians, and θ is the peak location. Increasing the annealing temperature increases the crystallite size value, leading to larger grain morphology. Table 2 summarizes the characteristics, including crystallite size, full width at half maximum

(FWHM), and position angle examines the influence of different annealing temperatures on the structural features of NiO films. The FWHM decreased from 0.3607° to 0.2509° , indicating that the crystal formation of the NiO film is enhanced at rising temperatures, resulting in a crystallite size increase from 23 to 33 nm. It also explains the high degree of ordering and structural improvement of crystallization—in other words, when the intensity is increased, the FWHM is minimal and vice versa (Takko et al., 2021). Throughout this investigation, it is considered that the crystallite size increases as the annealed temperature increases. In order to gain a deeper knowledge of the structural characteristics of the materials, we utilized Williamson-Hall (W-H) analysis. The Williamson-Hall (W-H) equation (Equation 2) was used to figure out the size of the crystallites and the microstrain from the width of the principal XRD peak intensity (Serin et al., 2017; Yildiz et al., 2015):

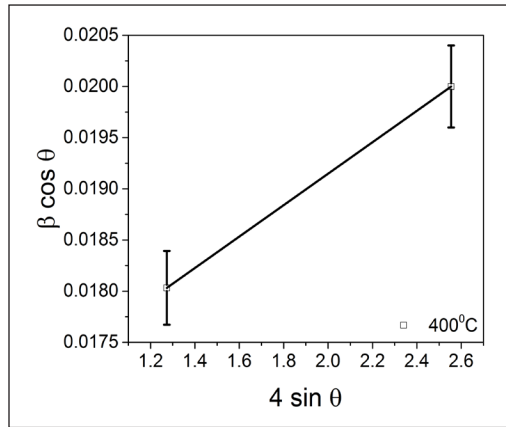
$$\beta_{hkl} = (0.9\lambda / D) + 4\epsilon \sin \theta \quad [2]$$

in which D is the crystallite size (nm), λ is the radiation wavelengths (here, $\text{CuK}\alpha$), β_{hkl} is the FWHM of the principal peak intensity, ϵ refers to the microstrain that is caused to flaws inside the crystalline lattice, and θ is the diffraction angle. Plots of the $\beta \cos \theta$ versus $4 \sin \theta$ for the preferred orientation peaks of the samples are depicted in Figure 5. The graph displayed a positive strain for the samples as the annealing temperature increased. The findings of the crystallite size derived by the W-H equation are lower than Scherrer's due to peak narrowing induced by micro strain acquired by W-H analysis (Table 2). The findings show that as the annealing temperature rises from 400°C to 700°C , the crystallite size grows, and the microstrain decreases gradually. The smaller value of the microstrain implies that the thin films are more crystalline and have a low number of flaws. It means that annealing the film changes the way the atoms are arranged in the crystal lattice, which minimizes the lattice imperfections and enhances the overall quality of the crystals (Aswathy et al., 2020). The larger crystallite size and reduced microstrain in NiO for the sample annealed at 700°C thin film confirm the enhancement of crystalline quality. A similar observation also made by, Aswathy et al. (2020) obtained an average crystallite size of 19.68 nm with a microstrain of 1.03×10^{-3} at an annealing temperature of 600°C for NiO thin films produced by spin coating deposition techniques. Furthermore, as the temperature rises, the drop in the FWHM of the diffraction peaks leads to a reduction of the slope (c), showing that the strain in the NiO lattice declines progressively (Pagar & Shinde, 2021). The tensile stress in the films at high annealing temperatures tends to cause the microstrain to change with increasing temperature (Jamal et al., 2019).

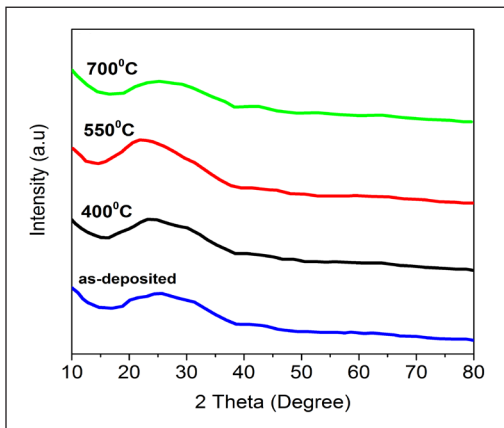
The XRD results of NiO films using Method II indicated only hollow peaks, as shown in Figure 4(b). No diffraction peaks occurred even after increasing the annealing temperature to 700°C . It indicates that the layer is in an amorphous phase containing a



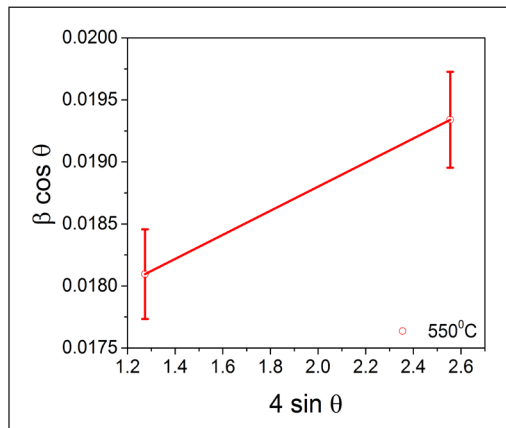
(a)



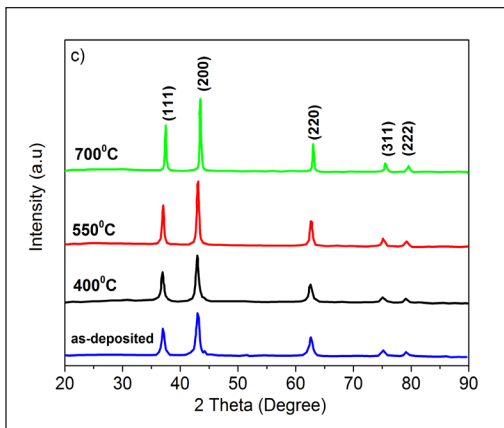
(a)



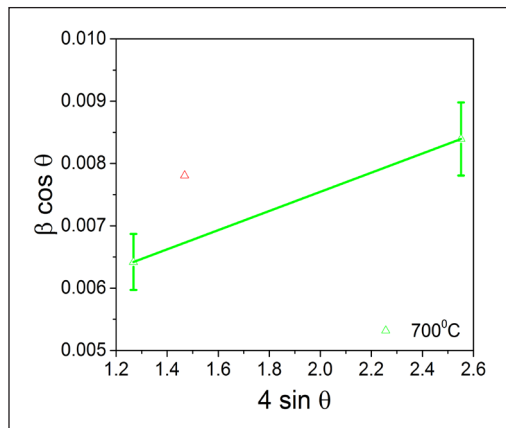
(b)



(b)



(c)



(c)

Figure 4. XRD pattern of NiO thin film by (a) Method I, (b) Method II, and (c) Method III at different annealing temperatures (400°C, 550°C, and 700°C)

Figure 5. The WH analysis for the NiO thin film by Method I (a) 400°C, (b) 550°C, and (c) 700°C. Solid lines represent best-fitting lines, while error bars represent standard deviations

Table 2
Structural parameter for (111) plane of the NiO thin film properties by Method I, Method II, and Method III

Annealing Temperature	hkl plane	2 Theta (degree)	FWHM	$c \times 10^{-2}$ (nm)	^a Crystallite size (nm)	^b Crystallite size (nm)	$\epsilon \times 10^{-3}$
Method I							
400°C	(111)	37.28	0.3607	1.80	23.24	7.67	0.74
550°C	(111)	37.05	0.2844	0.52	29.46	26.56	1.05
700°C	(111)	37.05	0.2509	0.55	33.40	33.25	1.00
Method II							
400°C	-	-	-	-	-	-	-
550°C	-	-	-	-	-	-	-
700°C	-	-	-	-	-	-	-
Method III							
As-deposited	(111)	37.0	0.2175	0.93	38.52	15.00	1.03
400°C	(111)	37.0	0.2175	0.61	38.52	22.77	1.02
550°C	(111)	37.2	0.1388	0.43	60.39	32.02	2.21
700°C	(111)	37.5	0.1171	0.32	71.64	43.06	1.19

^aFrom Scherrer's equation

^bFrom Williamson-Hall (WH) analysis

solvent agent or nickel salt. A lack of ordered internal structure in the amorphous phase in which the atoms and molecules are not arranged in a specific lattice pattern results in broader diffraction peaks instead of high-intensity narrower peaks. It may attribute to the modification of solvent material which used ethanol instead of 2-methoxyethnaol. Furthermore, as described in (Hajakbari, 2020), the XRD patterns show that the NiO thin films contain a single cubic crystal arrangement. Nevertheless, a wide peak at $2\theta = 24^\circ$ may be seen, corresponding to the quartz substrate. Similar patterns demonstrating the impact of annealing were achieved for silver, molybdenum oxide, and zirconium oxide thin films (Lupo et al., 2020). The XRD peaks were broad when the annealing temperature was raised, which was attributable to an improvement in particle size and crystallinity. The FWHM was seen to drop with annealing temperature, which might be attributed to a change in the concentration of lattice defects.

In the process of Method III, NiO films had five main prominent peaks of 37.2° , 43.2° , 62.8° , 75.4° , and 79° of 2 theta angle corresponding to the crystal plane of NiO (1 1 1), (2 0 0), (2 2 0), (3 1 1) and (2 2 2). The values “d” produced are equivalent to the NiO cubic phase with $a=b=c=4.170 \text{ \AA}$. The diffracted intensity for the planes of (1 1 1), (2 0 0), and (2 2 0) keep increasing sharply with an increasing annealing temperature, as observed in Figure 4(c). As in Method I, the high diffraction peak was observed at (111) for all the samples and obtained the average crystallite size. The crystallite size increased from 38 to 71 nm using Scherrer's equation and 15 to 43 nm using the W-H equation—the nickel

oxidation bond deficiencies on the bounds of grain with enhanced annealing temperature from 400°C to 700°C. Compared with the findings given in the journals, Ramesh et al. (Mulik, 2019), the findings available in different crystallite sizes were determined to be between 40 to 52 nm. The increasing annealed temperature provides crystallites with more energy that transfers them into permanent balance sites, resulting in the improvement of the crystallinity of NiO (Yang et al., 2019). Similar to Method I, a positive strain is obtained as the annealing temperature increases from 400°C to 700°C, illustrated in Figure 6. The strain of the sample decreases slowly as the as-deposited sample is annealed to 400°C. Subsequently, a quick rise in the strain value was observed at 550°C temperature and decreased as it reached 700°C, indicating a lower number of lattice imperfections. It could be due to the increasing temperature; the film becomes thick and lacks cracks and voids, allowing for faster crystal development (Jamal et al., 2019; Kumar et al., 2017).

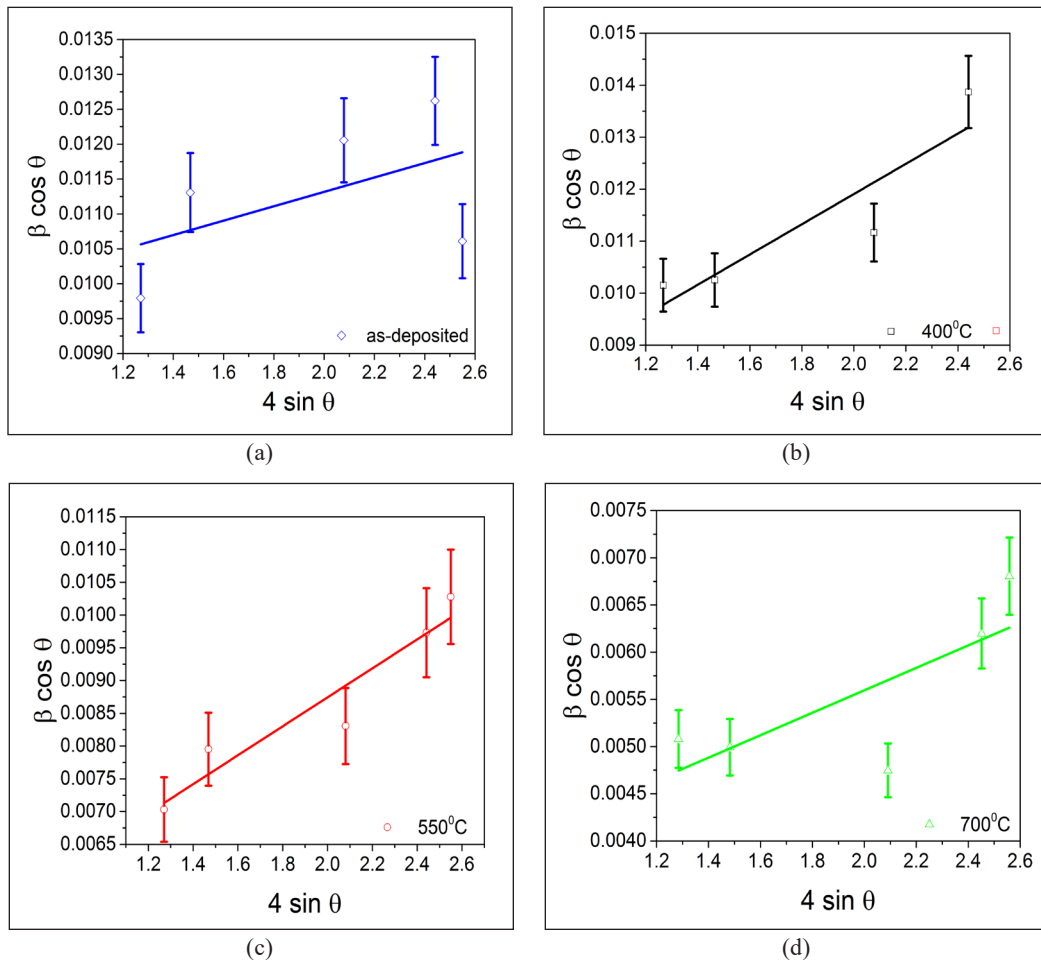


Figure 6. The WH analysis for the NiO thin film by Method III (a) as-deposited, (b) 400°C, (c) 550°C, and (d) 700°C. Solid lines represent best-fitting lines, while error bars represent standard deviations

Morphological Analysis

As illustrated in Figure 7, nanoparticles of green color NiO become black during the annealing process, which can be related to the previous results (Renaud et al., 2013), leading to a shortage or existence of nickel vacancy. The black-colored NiO films were subsequently transformed to bleach, with the rise in the annealing temperatures. The NiO thin films using Method I are thermally treated at various temperatures to study the surface morphology using SEM, as seen in Figure 8(a), with a magnification of 10,000. The NiO films comprise nanocrystalline grain, including a flat homogeneous substrate surface covered with top viewpoint for the films by the micrographs. The higher the temperature of the films, the more grains grew, and the condition of the films improved. It might be attributed to an enhancement in adatoms' thermal energy, which speeds up the migration of

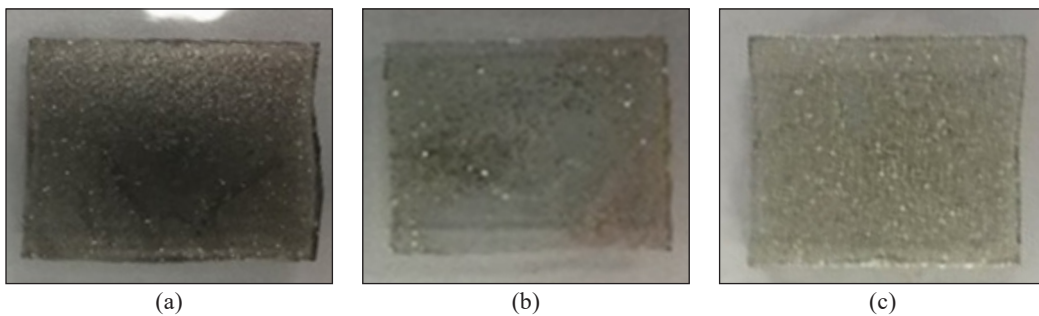


Figure 7. NiO films after annealed at (a) 400°C (b) 550°C (c) 700°C

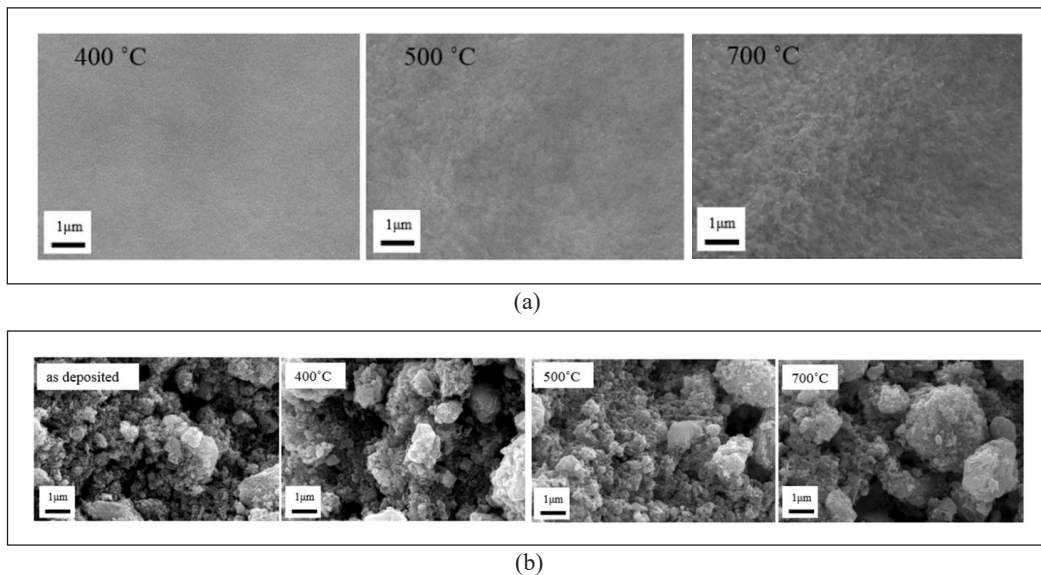


Figure 8. Surface morphologies performed at a magnification of 10.00kX annealed at different temperatures (400°C, 550°C, and 700°C) obtained from (a) Method I and (b) Method II

adatoms to favorable nucleation and growth sites, resulting in larger grain sizes. Christian et al. (Lupo et al., 2020) observed comparable SEM results for NiO films. However, there are a few small fractures discovered throughout the layer. It might be owing to the higher annealing temperatures utilized. The annealed temperature is considered to affect the interface structure of NiO films. The increased annealing temperature has a significant effect on the crystallite size of NiO (Haider et al., 2019; Yazdani et al., 2018).

SEM analysis was also conducted for the NiO films from Method III at various annealing temperatures [Figure 8 (b)]. The nanoparticles of NiO used in Method III were cubical and spherical. It can be seen that atoms are linked to one another from agglomerated particles. As the annealing temperature rose from 400°C to 550°C, the grains grew, indicating that the NiO films' structure had improved, as validated by the XRD results. It is clearly shown in Figure 8(b)) that certain bigger nanoparticles and strongly gathered when the annealing temperature is set to 700°C. A parallel finding was revealed in research (Wu et al., 2017), which suggested that this might be attributable to the large surface energy and the pressure of nanoparticles. The rise in grain size with raising the annealing temperature to 700°C indicates that the crystalline condition of the NiO film has improved. This increment is due to an expansion in the thermal energy of atoms, which promotes the movement of the atoms to appropriate nucleation and growing positions, leading to the formation of larger grains and an improvement in crystallinity. Bigger grain size results in transparent surfaces due to the decrease of grain borders and, as a result, fewer scatterings at the grain boundary (Sahoo & Thangavel, 2018).

Optical Properties

UV-Vis Spectroscopy was used to evaluate the produced NiO's optical characteristics, shown in Figure 9. The highest absorption peak of the NiO films in Method I was determined at a wavelength of about 336 nm. The absorption was greater than in the report presented by Ashique Kota and Hyung-Kee Seo (Kotta & Seo, 2019), who found absorption peaks at a wavelength of 321 nm. It might be owing to the various techniques and precursors employed. The optical energy band gaps of NiO were calculated by Tauc's equation (Equation 3) (Atak & Coşkun, 2017; Muniandy et al., 2021) based on the results from UV-Vis absorption spectra:

$$(\alpha h\nu)^n = A(h\nu - E_g) \quad [3]$$

where $h\nu$ is photo energy, α is absorption coefficient, and n is 2 for direct bandgap material. Based on the equation, it is possible to extrapolate the linear part of $(\alpha h\nu)^n$ to $h\nu$, i.e., to zero, to the optical band space for the absorption pitch. The band gap energy decreased at the higher annealing temperature from 3.6 to 3.1 eV. According to Patil et al. (2011), the

bandgap of the NiO materials annealed at 400°C to 700°C is decreased by 3.86 to 3.47 eV. The fall in deficient dimensions and the increase in particle size caused the decrease of E_g with a rising annealing temperature (Agbogou et al., 2018; Kayani et al., 2018; Muhammad et al., 2022). It is consistent with the results obtained from XRD analysis. According to XRD results, the crystallite size has increased as the annealing temperature increases. The increase in crystallite size indicated a decrease in the semiconductor's energy bandgap, similar to the findings reported by (Dwivedi et al. 2022; Muniandy et al., 2021; Kumar et al., 2017). Compared to bulk NiO (4.0eV), the produced samples exhibit lower E_g values. Consequently, the annealing temperature is inversely proportional to the energy band gap. The change in bandgap value may also be affected by several other variables, such as carrier concentrations, crystallite size, structural characteristics, impurity presence, and lattice strain (Dwivedi et al., 2022).

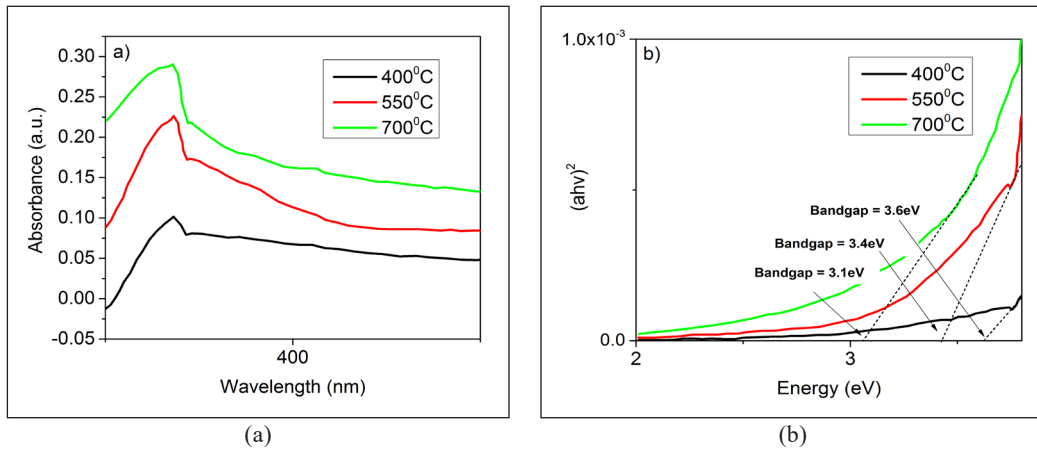


Figure 9. The method I result shows (a) the NiO spectrum of absorption from UV-Vis at various annealing temperatures (400°C, 550°C, and 700°C); (b) NiO thin sheet Tauc plot to measure the optical absorption.

The UV region of NiO film using Method II exhibited the highest absorption at about 339nm, although the XRD results did not prevail at any peaks. In addition, with the increasing annealing temperature from 400°C to 700°C, as indicated in Figure 10, the absorption factor of films increased. It might be due to an improvement in hole density with increasing annealing temperature. The higher the annealing temperature, the band gaps were observed to drop from 3.5 to 2.7eV. The decrease in the bandgap with an increased temperature may be due to crystalline growth and even to a decrease in the interface zone. According to the XRD findings, the grain size increased as the temperature increased. As grain size expanded, the density of the grain limit of the film decreased, and carriers at grain boundaries became less dispersed (Aftab et al., 2021).

Figure 11 shows the highest absorption peaks of NiO thin films using Method III in the UV region at about 339 nm wavelength. The absorbance coefficient of annealed

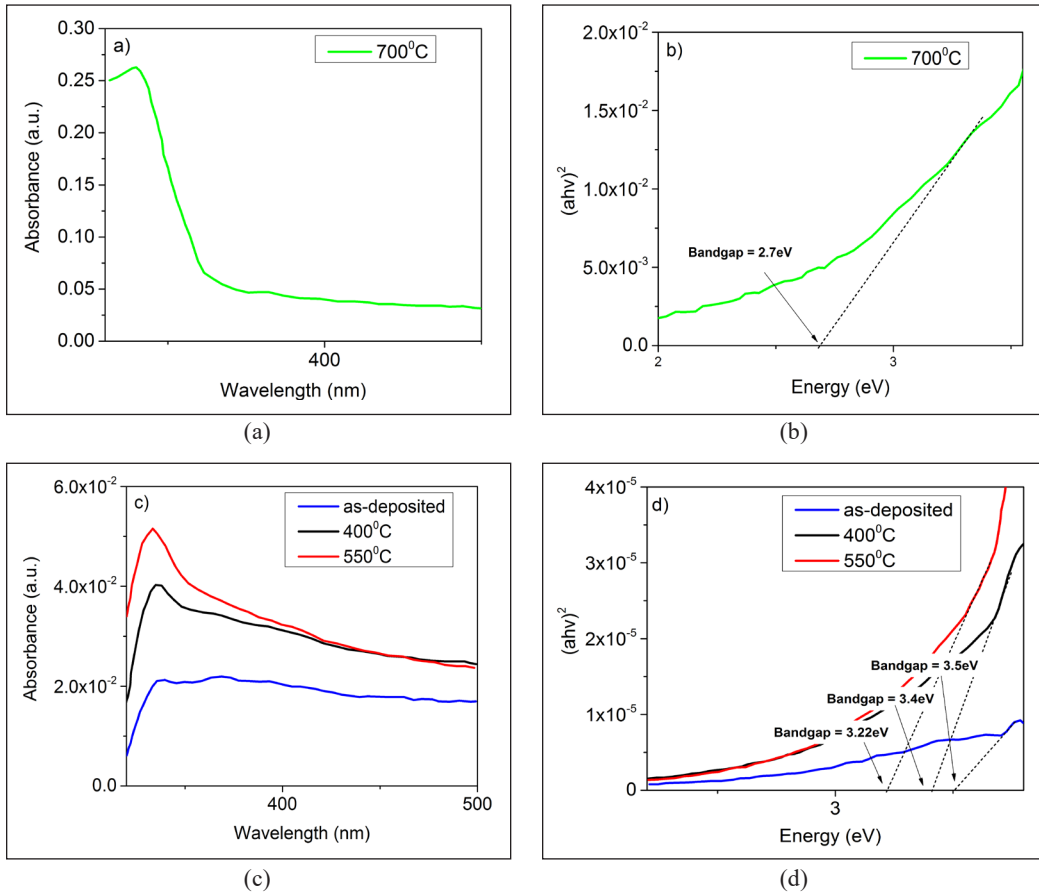


Figure 10. Method II outcome of NiO film (a) UV-Vis absorption spectrum at a temperature of 700°C, (b) Tauc plot for the evaluation of the optical bandgap at 700°C, (c) UV-Vis absorption spectrum at a different annealing temperature of the films (as-deposited, 400°C, and 550°C), and (d) Tauc plot of thin films at various temperatures for the optical bandgap (as-deposited, 400°C, and 550°C)

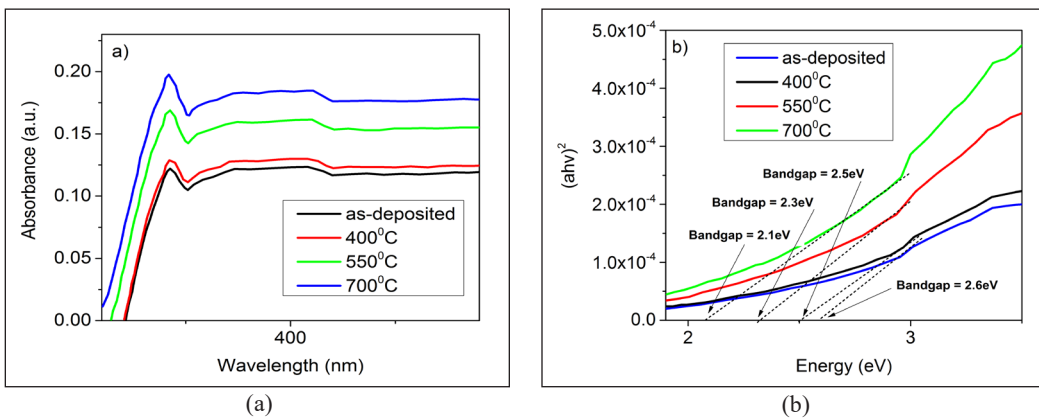


Figure 11. Method III outcome indicates (a) the NiO spectrum of absorptions at various temperatures (400°C, 550°C, and 700°C), and (b) a Tauc plot to evaluate the optical band gap

films increases as the annealing temperature rises, comparable to Method I and II. The absorbance coefficient of films annealed at a lower temperature (400°C) is less than that of films annealed at a higher temperature. The NiO films at 700°C efficiently absorbed photon energy and displayed greater absorption in the UV band when contrasted to the as-deposited and lower temperatures. According to the Tauc displayed graph, the bandgap decreases from 2.38 to 2.15 eV when the annealing temperature increases from 400°C to 700°C. It resists chemical flaws or vacancies in the crystal structure, reducing bandgap energy. The fall in energy from the bandgap can be associated with increasing grain size and decreasing concentration of defect sites that lead to reduced defect. The bandgap may therefore be determined directly by the size of the grain.

CONCLUSION

The NiO nanoparticles were synthesized with three different precursors and deposited using the spin coating. Method I, II, and III samples were annealed at different temperatures (400°C, 550°C, and 700°C). The NiO thin films were studied in detail according to the results obtained from XRD, SEM, and UV-Vis spectroscopy. Comparing these three methods, Method I have shown more potential to be an HTL layer resulting in increasing crystallite size, reducing microstrain, uniform surface of the film with the absence of agglomerated particles and pin-hole free, and decreasing bandgap energies. The thermal treatment considerably impacts the structures' forms, sizes, and energy band gap. The XRD result revealed that when the annealing temperature increased, the crystallite size of the NiO thin film also increased from 23 to 71 nm obtained from Scherrer's equation and 7.6 to 43 nm attained from Williamson-Hall's (WH) equation. An excellent diffract intensity of NiO was demonstrated using Methods I and III. Nevertheless, only hollow peaks were found from Method II, even annealed after increasing the annealing temperature to 700°C. The surface morphology of Method I NiO thin film exhibited a denser and uniform surface in contrast to Method III demonstrated agglomerated particles. Furthermore, the band gap energies were decreased from 3.60 to 2.10 eV with an increase in annealing temperature. Henceforth, the synthesis of NiO thin film performed well at the annealing temperature of 700°C, the crystallinity of NiO has enhanced owing to its greater absorption coefficient, uniform, and pinhole-free surface area, fast deposition crystallization, and a lower number of lattice imperfections occur due to the size and microstrain which aspects that proposed NiO as a good candidate for HTM.

ACKNOWLEDGEMENT

This work was supported by the Ministry of Higher Education Malaysia and Universiti Teknikal Malaysia Melaka through the Fundamental Research Grant Scheme with Project No PJP/2021/FTKEE/S01822 and FRGS/1/2020/FKEKK-CETRI/F00423.

REFERENCES

- Abbas, M., Zeng, L., Guo, F., Rauf, M., Yuan, X. C., & Cai, B. (2020). A critical review on crystal growth techniques for scalable deposition of photovoltaic perovskite thin films. *Materials*, *13*(21), Article 4851. <https://doi.org/10.3390/ma13214851>
- Aftab, M., Butt, M. Z., Ali, D., Bashir, F., & Khan, T. M. (2021). Optical and electrical properties of NiO and Cu-doped NiO thin films synthesized by spray pyrolysis. *Optical Materials*, *119*, Article 111369. <https://doi.org/10.1016/j.optmat.2021.111369>
- Agbogu, A. N. C., Orji, M. P., & Ekwealor, A. B. C. (2018). Investigations into the influence of temperature on the optical properties of NiO thin films. *Indian Journal of Pure and Applied Physics*, *56*(2), 136-141.
- Aswathy, N. R., Varghese, J., & Vinodkumar, R. (2020). Effect of annealing temperature on the structural, optical, magnetic and electrochemical properties of NiO thin films prepared by sol-gel spin coating. *Journal of Materials Science: Materials in Electronics*, *31*, 16634-16648. <https://doi.org/10.1007/s10854-020-04218-5>
- Atak, G., & Coşkun, Ö. D. (2017). Annealing effects of NiO thin films for all-solid-state electrochromic devices. *Solid State Ionics*, *305*, 43-51. <https://doi.org/10.1016/j.ssi.2017.05.002>
- Atli, A., Atilgan, A., Altinkaya, C., Ozel, K., & Yildiz, A. (2019). St. Lucie cherry, yellow jasmine, and madder berries as novel natural sensitizers for dye-sensitized solar cells. *International Journal of Energy Research*, *43*(8), 3914-3922. <https://doi.org/10.1002/er.4538>
- Atli, A., Atilgan, A., & Yildiz, A. (2018). Multi-layered TiO₂ photoanodes from different precursors of nanocrystals for dye-sensitized solar cells. *Solar Energy*, *173*, 752-758. <https://doi.org/10.1016/j.solener.2018.08.027>
- Desissa, T. D. (2021). NiO-ZnO based junction interface as high-temperature contact materials. *Ceramics International*, *47*(6), 8053-8059. <https://doi.org/10.1016/j.ceramint.2020.11.159>
- Du John H, V., Moni D, J., & Gracia, D. (2020). A detailed review on Si, GaAs, and CIGS/CdTe based solar cells and efficiency comparison. *Przeгляд Elektrotechniczny*, *96*(12), 9-18. <http://dx.doi.org/10.15199/48.2020.12.02>
- Dwivedi, S., Nayak, H. C., Parmar, S. S., Kumhar, R. P., & Rajput, S. (2022). Calcination temperature reflected structural, optical and magnetic properties of nickel oxide. *Magnetism*, *2*(1), 45-55. <https://doi.org/10.3390/magnetism2010004>
- Ebhota, W. S., & Jen, T. C. (2020). Fossil fuels environmental challenges and the role of solar photovoltaic technology advances in fast tracking hybrid renewable energy system. *International Journal of Precision Engineering and Manufacturing-Green Technology*, *7*, 97-117. <https://doi.org/10.1007/s40684-019-00101-9>
- Gil, B., Yun, A. J., Lee, Y., Kim, J., Lee, B., & Park, B. (2019). Recent progress in inorganic hole transport materials for efficient and stable perovskite solar cells. *Electronic Materials Letters*, *15*, 505-524. <https://doi.org/10.1007/s13391-019-00163-6>
- Guo, Y., Yin, X., & Que, W. (2017). NiO_x mesoporous films derived from Ni(OH)₂ nanosheets for perovskite solar cells. *Journal of Alloys and Compounds*, *722*, 839-845. <https://doi.org/10.1016/j.jallcom.2017.06.185>

- Haider, A. J., Al-Anbari, R., Sami, H. M., & Haider, M. J. (2019). Photocatalytic activity of nickel oxide. *Journal of Materials Research and Technology*, 8(3), 2802-2808. <https://doi.org/10.1016/j.jmrt.2019.02.018>
- Hajakbari, F, Afzali, M. T., & Hojabri, A. (2017). Nanocrystalline nickel oxide (NiO) thin films grown on quartz substrates: Influence of annealing temperatures. *Acta Physica Polonica A*, 131(3), 417-419. <https://doi.org/10.12693/APhysPolA.131.417>
- Hajakbari, F. (2020). Characterization of nanocrystalline nickel oxide thin films prepared at different thermal oxidation temperatures. *Journal of Nanostructure in Chemistry*, 10(1), 97-103. <https://doi.org/10.1007/s40097-020-00332-2>
- Ibn-Mohammed, T., Koh, S. C. L., Reaney, I. M., Acquaye, A., Schileo, G., Mustapha, K. B., & Greenough, R. (2017). Perovskite solar cells: An integrated hybrid lifecycle assessment and review in comparison with other photovoltaic technologies. *Renewable and Sustainable Energy Reviews*, 80, 1321-1344. <https://doi.org/10.1016/j.rser.2017.05.095>
- Jamal, M. S., Shahahmadi, S. A., Chelvanathan, P., Alharbi, H. F., Karim, M. R., Dar, M. A., Luqman, M., Alharthi, N. H., Al-Harhi, Y. S., Aminuzzaman, M., Asim, N., Sopian, K., Tiong, S. K., Amin, N., & Akhtaruzzaman, M. (2019). Effects of growth temperature on the photovoltaic properties of RF sputtered undoped NiO thin films. *Results in Physics*, 14, Articles 102360. <https://doi.org/10.1016/j.rinp.2019.102360>
- Kayani, Z. N., Butt, M. Z., Riaz, S., & Naseem, S. (2018). Synthesis of NiO nanoparticles by sol-gel technique. *Materials Science-Poland*, 36(4), 547-552. <https://doi.org/10.2478/msp-2018-0088>
- Kotta, A., & Seo, H.-K. (2019). Nickel Oxide Monodispersed Quantum Dots as Hole Transport Layer in *n-i-p* Hybrid Perovskite Solar Cells. *Journal of Nanoelectronics and Optoelectronics*, 14(7), 895-899. <https://doi.org/10.1166/jno.2019.2660>
- Li, M. H., Yum, J. H., Moon, S. J., & Chen, P. (2016). Inorganic p-type semiconductors: Their applications and progress in dye-sensitized solar cells and perovskite solar cells. *Energies*, 9(5), Article 331. <https://doi.org/10.3390/en9050331>
- Li, S., Cao, Y. L., Li, W. H., & Bo, Z. S. (2021). A brief review of hole transporting materials commonly used in perovskite solar cells. *Rare Metals*, 40, 2712-2729. <https://doi.org/10.1007/s12598-020-01691-z>
- Lupo, C., Eberheim, F., & Schlettwein, D. (2020). Facile low-temperature synthesis of nickel oxide by an internal combustion reaction for applications in electrochromic devices. *Journal of Materials Science*, 55, 14401-14414. <https://doi.org/10.1007/s10853-020-04995-8>
- Luszczek, M., Łuszczek, G., & Świsulski, D. (2021). Simulation investigation of perovskite-based solar cells. *Przełąd Elektrotechniczny*, 2021(5), 99-102. <https://doi.org/10.1109/ECACE.2019.8679283>
- Mariotti, N., Bonomo, M., Fagiolari, L., Barbero, N., Gerbaldi, C., Bella, F., & Barolo, C. (2020). Recent advances in eco-friendly and cost-effective materials towards sustainable dye-sensitized solar cells. *Green Chemistry*, 22, 7168-7218. <https://doi.org/10.1039/D0GC01148G>
- Mohammadian-Sarcheshmeh, H., Arazi, R., & Mazloum-Ardakani, M. (2020). Application of bifunctional photoanode materials in DSSCs: A review. *Renewable and Sustainable Energy Reviews*, 134, Article 110249. <https://doi.org/10.1016/j.rser.2020.110249>

- Muhammad, S., Nomaan, A. T., Idris, M. I., & Rashid, M. (2022). Structural, optical and electrical investigation of low-temperature processed zinc oxide quantum dots based thin films using precipitation-spin coating on flexible substrates. *Physica B: Condensed Matter*, 635, Article 413806. <https://doi.org/10.1016/j.physb.2022.413806>
- Mulik, R. N. (2019). Microstructural studies of nanocrystalline nickel oxide. *International Journal Of Research And Analytical Reviews*, 6(2), 973-981. <https://doi.org/10.1063/1.4802404>
- Muniandy, S., Idris, M. I. B., Napiah, Z. A. F. B. M., Yusof, H. H. M., Chachuli, S. A. M., & Rashid, M. (2021). An investigation on NiO for hole transport material in perovskite solar cells. In *2021 IEEE Regional Symposium on Micro and Nanoelectronics (RSM)* (pp. 112-115). IEEE Publishing. <https://doi.org/10.1109/RSM52397.2021.9511573>
- Nkele, A. C, Nwanya, A. C, Shinde, N. M., Ezugwu, S., Maaza, M., Shaikh, J. S., & Ezema, F. I. (2020). The use of nickel oxide as a hole transport material in perovskite solar cell configuration: Achieving a high performance and stable device. *International Journal of Energy Research*, 44(13), 9839-9863. <https://doi.org/10.1002/er.5563>
- Pagar, U., & Shinde, U. P. (2021). Annealing effect on structural, morphological and electrical properties by screen printed bunsenite NiO thick films. *International Journal of Innovative Technology and Exploring Engineering*, 10(6), 80-85. <https://doi.org/10.35940/ijitee.F8826.0410621>
- Park, H. H. (2021). Efficient and stable perovskite solar cells based on inorganic hole transport materials. *Nanomaterials*, 12(1), Article 112. <https://doi.org/10.3390/nano12010112>
- Patil, V. P., Pawar, S., Chougule, M., Godse, P., Sakhare, R., Sen, S., & Joshi, P. (2011). Effect of annealing on structural, morphological, electrical and optical studies of nickel oxide thin films. *Journal of Surface Engineered Materials and Advanced Technology*, 1(2), 35-41. <https://doi.org/10.4236/jsemat.2011.12006>
- Pitaro, M., Tekelenburg, E. K., Shao, S., & Loi, M. A. (2022). Tin halide perovskites: From fundamental properties to solar cells. *Advanced Materials*, 34(1), Article 2105844. <https://doi.org/10.1002/adma.202105844>
- Renaud, A., Chavillon, B., Cario, L., Pleux, L. Le, Szuwarski, N., Pellegrin, Y., Blart, E., Gautron, E., Odobel, F., & Jobic, S. (2013). Origin of the black color of NiO used as photocathode in p-type dye-sensitized solar cells. *Journal of Physical Chemistry C*, 117(44), 22478-22483. <https://doi.org/10.1021/jp4055457>
- Roy, A., Ghosh, A., Bhandari, S., Sundaram, S., & Mallick, T. K. (2020). Perovskite solar cells for BIPV application: A review. *Buildings*, 10(7), Article 129. <https://doi.org/10.3390/buildings10070129>
- Sahoo, P., & Thangavel, R. (2018). Effect of annealing temperature on physical properties of solution processed nickel oxide thin films. In *AIP Conference Proceedings* (Vol. 1961, p. 30041). AIP Publishing LLC. <https://doi.org/10.1063/1.5035243>
- Kumar, R. S., Johnson Jeyakumar, S., Jothibas, M., Kartharinal Punithavathy, I., & Prince Richard, J. (2017). Influence of molar concentration on structural, optical and magnetic properties of NiO nanoparticles. *Journal of Materials Science: Materials in Electronics*, 28(20), 15668-15675.
- Serin, T., Atilgan, A., Kara, I., & Yildiz, A. (2017). Electron transport in Al-Cu co-doped ZnO thin films. *Journal of Applied Physics* (Vol. 121, No. 9, p. 95303). AIP Publishing LLC. <https://doi.org/10.1063/1.4977470>

- Shariatinia, Z. (2020). Recent progress in development of diverse kinds of hole transport materials for the perovskite solar cells: A review. *Renewable and Sustainable Energy Reviews*, 119, Article 109608. <https://doi.org/10.1016/j.rser.2019.109608>
- Takko, S. Y., Amin, B. D. E., Y, C. I., & Shekarau, J. I. (2021). Crystallinity, amorphousity and characterization of synthesized Sb_2O_3 , BaO and NiO nanoparticles and nanocomposites. *International Journal of Innovative Science and Research Technology*, 6(11), 822-831.
- Wang, H., Yu, Z., Jiang, X., Li, J., Cai, B., Yang, X., & Sun, L. (2017). Efficient and stable inverted planar perovskite solar cells employing CuI as hole-transporting layer prepared by solid-gas transformation. *Energy Technology*, 5(10), 1836-1843. <https://doi.org/10.1002/ente.201700422>
- Wang, K., Tian, Y., Jiang, H., Chen, M., & Xu, S. (2019). Surface treatment on nickel oxide to enhance the efficiency of inverted perovskite solar cells. *International Journal of Photoenergy*, 2019, Article 4360816. <https://doi.org/10.1155/2019/4360816>
- Wilson, G. M., Al-Jassim, M., Metzger, W. K., Glunz, S. W., Verlinden, P., Xiong, G., Mansfield, L. M., Stanbery, B. J., Zhu, K., Yan, Y., Berry, J. J., Ptak, A. J., Dimroth, F., Kayes, B. M., Tamboli, A. C., Peibst, R., Catchpole, K., Reese, M. O., Klinga, C. S., ... & Sulas-Kern, D. B. (2020). The 2020 photovoltaic technologies roadmap. *Journal of Physics D: Applied Physics*, 53(49), Article 493001. <https://doi.org/10.1088/1361-6463/ab9c6a>
- Wu, J., Lan, Z., Lin, J., Huang, M., Huang, Y., Fan, L., Luo, G., Lin, Y., Xie, Y., & Wei, Y. (2017). Counter electrodes in dye-sensitized solar cells. *Chemical Society Reviews*, 46(19), 5975-6023. <https://doi.org/10.1039/C6CS00752J>
- Yang, P., Li, L., Yu, S., Zheng, H., & Peng, W. (2019). The annealing temperature and films thickness effect on the surface morphology, preferential orientation and dielectric property of NiO films. *Applied Surface Science*, 493, 396-403. <https://doi.org/10.1016/j.apsusc.2019.06.223>
- Yang, W. F., Igbari, F., Lou, Y. H., Wang, Z. K., & Liao, L. S. (2020). Tin halide perovskites: Progress and challenges. *Advanced Energy Materials*, 10(13), Article 1902584. <https://doi.org/10.1002/aenm.201902584>
- Yazdani, A., Zafarkish, H., & Rahimi, K. (2018). The variation of Eg-shape dependence of NiO nanoparticles by the variation of annealing temperature. *Materials Science in Semiconductor Processing*, 74, 225-231. <https://doi.org/10.1016/j.mssp.2017.10.048>
- Yildiz, A., Cansizoglu, H., Abdulrahman, R., & Karabacak, T. (2015). Effect of grain size and strain on the bandgap of glancing angle deposited AZO nanostructures. *Journal of Materials Science: Materials in Electronics*, 26, 5952-5957. <https://doi.org/10.1007/s10854-015-3167-0>
- Yildiz, Abdullah, Chouki, T., Atli, A., Harb, M., Verbruggen, S. W., Ninakanti, R., & Emin, S. (2021). Efficient iron phosphide catalyst as a counter electrode in dye-sensitized solar cells. *ACS Applied Energy Materials*, 4(10), 10618-10626. <https://doi.org/10.1021/acsaem.1c01628>
- Yin, X., Guo, Y., Xie, H., Que, W., & Kong, L. B. (2019). Nickel oxide as efficient hole transport materials for perovskite solar cells. *Solar RRL*, 3(5), Article 1900001. <https://doi.org/10.1002/solr.201900001>
- Younas, M., Gondal, M. A., Dastageer, M. A., & Baig, U. (2019). Fabrication of cost effective and efficient dye sensitized solar cells with WO_3 - TiO_2 nanocomposites as photoanode and MWCNT as Pt-free counter electrode. *Ceramics International*, 45(1), 936-947. <https://doi.org/10.1016/j.ceramint.2018.09.269>